Combining Donor Strength and Oxidative Stability in Scorpionates: A Strongly Donating Fluorinated Mesoionic Tris(imidazol-5-ylidene)borate Ligand

Joseph S. Scott,† Joseph E. Schneider,† Eyob G. Tewelde, Joel G. Gardner, Sophie W. Anferov, Alexander S. Filatov, and John S. Anderson*

Department of Chemistry, University of Chicago, Chicago, IL 60637, USA

ABSTRACT: Strongly donating scorpionate ligands support the study of high-valent transition metal chemistry; however, their use is frequently limited by oxidative degradation. To address this concern, we report the synthesis of a tris(imidazol-5-ylidene)borate ligand featuring trifluoromethyl groups surrounding its coordination pocket. This ligand represents the first example of a chelating poly(imidazol-5-ylidene) mesoionic carbene ligand, a scaffold which is expected to be extremely donating. The {NiNO}^{10} complex of this ligand, as well as that of a previously reported strongly donating tris(imidazol-2-ylidene)borate, have been synthesized and characterized. This new ligand's strong donor properties, as measured by the υ_{NO} of its {NiNO}^{10} complex and natural bonding orbital second-order perturbative energy analysis, are on par with those of the well-studied alkyl substituted tris(imidazol-2-ylidene)borates which are known to effectively stabilize high-valent intermediates. The good donor properties of this ligand, despite the electron withdrawing trifluoromethyl substituents, arise from the strongly donating imidazol-5-ylidene mesoionic carbene arms. These donor properties, when combined with the robustness of trifluoromethyl groups towards oxidative decomposition, suggest this ligand scaffold will be a useful platform in the study of oxidizing high-valent transition metal species.

Introduction

The oxidative chemistry of high-valent transition metal intermediates, particularly those featuring metal–ligand multiple bonds (e.g. oxos, nitrenes), is central in globally important transformations such as biological substrate oxidation,[1–6] synthetic C–H bond cleavage and functionalization,[7–16] and water oxidation.[17–23] This importance has spurred an enormous amount of effort toward generating model complexes or discrete intermediates for detailed characterization and study. Despite the need for well-defined model complexes, many useful ligand classes, such as phosphines, are better suited to stabilizing low-valent intermediates as opposed to high-valent, oxidizing species. In fact, recent work has called out the need for more oxidatively stable ligand scaffolds to advance our understanding of oxidizing intermediates.[24–26] There are many examples where oxidative ligand degradation continues to be a challenge,[27–33] with intramolecular oxidation of pendant C–H bonds being a particularly common mode of degradation.[34–45]

Tripodal tris-carbene based scaffolds are a class of ligands known to form oxidatively robust M–C bonds, promote low coordination environments, and stabilize high oxidation state compounds (Figure 1A).[45–59] The utility of these ligands arises in part from their strong donating ability, as measured by the N–O stretching frequency (υ_{NO}) of their four-coordinate {NiNO}^{10} complexes (Feltham-Enemark notation).[60,61] Our recent studies of Co-oxo complexes supported by tris(carbene)borate ligands have revealed ligand oxidation upon generation of an oxidizing

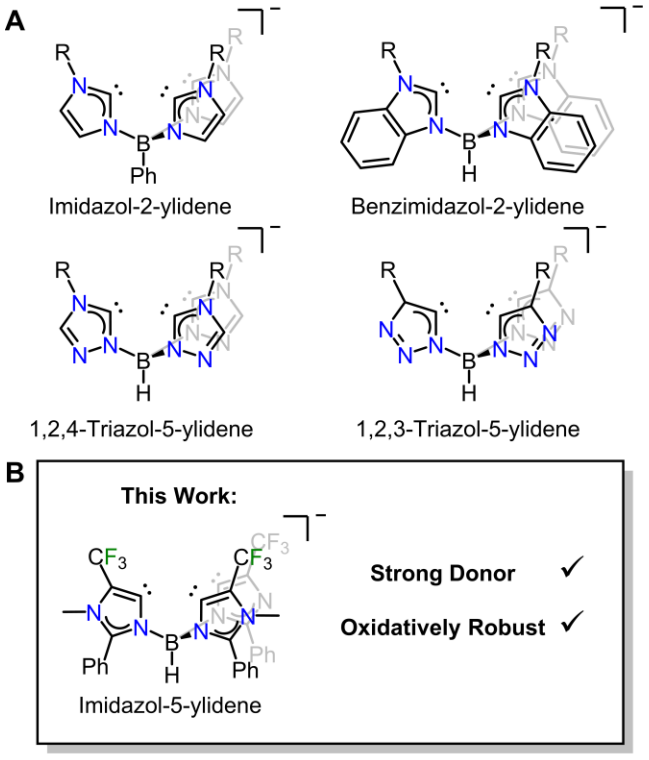

Figure 1. (**A**) Tris(carbene)borate ligands, some of which have been implemented in the stabilization and isolation of compounds with high oxidation states. (**B**). A tris(imidazole-5-ylidene)borate ligand, HB(^{CF3}mIm)$^-$, with trifluoromethyl groups surrounding its coordination pocket, introduced in this work.

$[PhB(^{Ad}Im)_3Co^{IV}O]^+$ intermediate, resulting in the hydroxylation of an aliphatic C–H bond on a ligand arm.[45] This observation further underscores how preventing ligand C–H oxidation is a major challenge in stabilizing highly oxidizing intermediates.

One way to address this problem is utilizing fluorinated ligands. Replacing oxidatively vulnerable C–H bonds with inert C–F bonds eliminates oxidative ligand degradation pathways, thus improving and sometimes promoting intermolecular reactivity.[62–67] We therefore envisioned installing perfluoroalkyl groups at the β-positions surrounding the coordination pocket in a tris(carbene)borate scaffold as a strategy to support highly oxidizing intermediates. However, these electron withdrawing groups should substantially decrease the donor strength of the ligand,[68] and so we targeted fluorinated imidazol-5-ylidene donors (Figure 1B). These carbenes, also known as mesoionic or abnormal N-heterocyclic carbenes (aNHCs),[69] are known to be better σ-donors than the classic Arduengo-type imidazol-2-ylidenes.[70–72] We hypothesized that functionalizing these more donating carbenes with electron-withdrawing perfluoroalkyl groups could facilitate a "Goldilocks" scenario in which an oxidatively stable ligand has donor strength comparable to the well-studied tris(imidazol-2-ylidene)borates.

Herein we report the synthesis of such a ligand — a tripodal, tris(imidazol-5-ylidene)borate with trifluoromethyl groups at the β carbon (4-position). This ligand, $HB(^{CF3}mIm)_3^-$, remains strongly donating despite the incorporation of oxidatively robust but electron withdrawing trifluoromethyl groups. To assess the donor properties of the ligand, we synthesized, characterized, and measured the N–O stretching frequency (υ_{NO}) of the corresponding $\{NiNO\}^{10}$ complex (**1**) of the ligand, alongside that of the strongly donating tris(imidazol-2-ylidene)borate ligand $PhB(^{Ad}Im)_3^-$ (**2**). We compare the υ_{NO} of these complexes to those of previously analyzed $\{NiNO\}^{10}$ complexes of tris(carbene)borate ligands.[60,73–75] Additionally, we used density functional theory (DFT) and natural bonding orbital (NBO) calculations to further analyze the donor properties in complexes **1**, **2**, $PhB(^{tBu}Im)_3NiNO$ (**3**), and two theoretical complexes: the imidazol-2-ylidene congener of **1** ($\mathbf{1_{NHC}}$) and the non-fluorinated congener of **1** ($\mathbf{1_{CH3}}$). We find that $HB(^{CF3}mIm)_3^-$ has a donor strength comparable to that of alkyl-substituted tris(imidazol-2-ylidene)borate ligands, and computations confirm that the electron-withdrawing effect of the trifluoromethyl groups is balanced by the innately strong donor strength of the mesoionic carbenes. These results suggest this platform is promising for the isolation of highly-oxidized transition metal intermediates.

Results and Discussion

*Synthesis and Characterization of $[HB(^{CF3}mImH)_3](OTf)_2$, **1**, and **2***

The trifluoromethylated ligand arm is synthesized using an *in situ* generated trifluoromethylated iodoxy reagent following a modified literature procedure.[76] The proligand $[HB(^{CF3}mImH)_3](OTf)_2$ is then assembled using standard substitution chemistry with $HBBr_2{\bullet}SMe_2$ and TMSOTf, employing conditions similar to those previously used to synthesize imidazolyl scorpionate proligands.[73] Assembly was

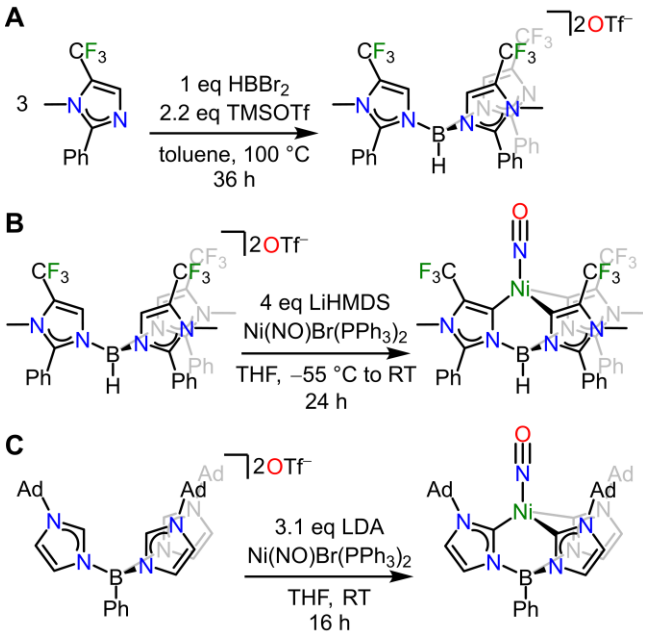

Scheme 1. (**A**) Synthesis of $[HB(^{CF3}mImH)_3](OTf)_2$, (**B**) complex **1**, and (**C**) complex **2**.

verified by multinuclear NMR spectroscopy and elemental analysis (Scheme 1A, see SI). NMR spectroscopy highlights the compound's trigonal symmetry, and its ^1H NMR spectrum features a downfield resonance at δ 7.88 ppm which can be assigned to the comparatively acidic imidazolium protons. The $^1J_{CH}$ of this proton is 205 Hz, suggesting that its corresponding tris(carbene)borate should be similarly donating to $PhB(^{Ad}Im)_3^-$ ($^1J_{CH}$ = 217 Hz, Figure S3 and S12).[79,80]

We then sought to metalate this new platform. We reasoned that a κ^3 Ni nitrosyl complex would be a compelling target; $\{NiNO\}^{10}$ complexes have been isolated with a variety of ligand scaffolds, and the υ_{NO} of these species can be used to measure the donor strength of scorpionate ligands.[60] Addition of LiHMDS (HMDS = hexamethyldisilazide) to a chilled slurry of $[HB(^{CF3}mImH)_3](OTf)_2$ in THF results in an orange-red solution. This deprotonated intermediate is temperature sensitive; solutions warmed above −35 °C turn dark reddish-brown. Similarly intense colors are observed with alternative bases such as KHMDS or lithium diisopropylamide (LDA), even at lower temperatures. The use of NaH also leads to mixtures of products (i.e. with free imidazole arm). The instability of this proposed deprotonated intermediate contrasts with previously reported tris(carbene)borates, many of which are deprotonated with LDA and can be observed by NMR at room temperature.[49,73,74] Despite this instability, $[HB(^{CF3}mImH)_3^-](OTf)_2$ can be effectively deprotonated and metalated via a stepwise procedure. Addition of 2.5 equivalents of LiHMDS at −55 °C with stirring for one hour is followed by addition to the $\{NiNO\}^{10}$ synthon $Ni(NO)Br(PPh_3)_2$ at room temperature and stirring for 4 hours. Subsequent addition of 1.5 equivalents of LiHMDS at −55 °C and slow warming overnight results in the formation of the desired metalated product $HB(^{CF3}mIm)_3NiNO$ as a red-orange solid in 20% yield (**1**, Scheme 1B). Addition of 3 or more equivalents of LiHMDS at the outset of the reaction, followed by transfer to $Ni(NO)Br(PPh_3)_2$, results in a

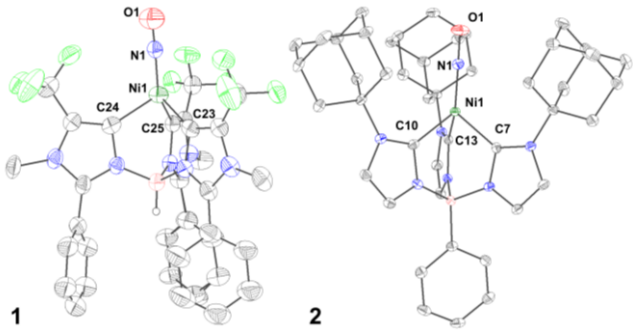

Figure 2. Crystal structures of complexes **1** and **2**. Thermal ellipsoids are shown at 50% probability. All H atoms besides that bound to B are omitted for clarity. Additional disordered parts have been omitted from the structure of **1**; a structure displaying the disorder is shown in Figure S26. Selected bond lengths (Å) and angles (deg) for **1**: Ni(1)−N(1) 1.671(1); Ni(1)−C(3/23) 1.973(6); Ni(1)−C(3/24) 1.973(6); Ni(1)−C(6/25) 1.987(8); N(1)− O(1) 1.14(2); C(3/23)−Ni(1)−C(3/24) 94.5(3); C(3/23)−Ni(1)−C(6/25) 91.6(2); C(3/24)−Ni(1)−C(6/25) 91.6(2); Ni(1)−N(1)−O(1) 175(3). Selected bond lengths (Å) and angles (deg) for **2**: Ni(1)−N(1) 1.657(3); Ni(1)−C(7) 1.997(3); Ni(1)−C(10) 1.993(3); Ni(1)−C(13) 1.962(3); N(1)− O(1) 1.183(4); C(7)−Ni(1)−C(10) 91.41(11); C(7)−Ni(1)−C(13) 93.46(11); C(10)−Ni(1)−C(13) 88.74(12); Ni(1)−N(1)−O(1) 175.7(3).

product mixture with higher amounts of unreacted ligand and a putative κ^2-product where only two of the ligand arms are bound to Ni (Figure S6).

Complex **1** is stable at ambient temperature in the solid state and in DMF solution, and it is also thermally stable up to 65 °C in acetonitrile (Figure S11). It was characterized by multinuclear NMR, single crystal X-ray diffraction (SXRD), and high-resolution mass spectrometry (HRMS, see SI). Trigonal symmetry is apparent in its NMR spectra (Figure S7-9), and a downfield metal-bound carbene resonance is observed at δ 180.2 ppm in its $^{13}C\{^1H\}$ NMR spectrum (Figure S8). The SXRD structure further supports the trigonal symmetry of **1** and confirms the bound NO and $HB(^{CF3}mIm)_3^-$ ligands (Figure 2). The SXRD structure is positionally disordered in both the Ph groups and the NO ligand (Figure S26). This disorder affects the final refinement precision and precludes detailed geometry comparisons. Nevertheless, the results are of sufficient quality for connectivity comparison between **1** and related complexes. We speculate that the positional disorder of the NO ligand may relate to a larger coordination pocket formed by the CF_3 groups in **1**.

We synthesized **1** in order to use its υ_{NO} as a measure of the donor strength of this new tris(imidazol-5-ylidene)borate ligand. Concurrently, we also sought a comparison at the limit of strongly donating tris(imidazol-2-ylidene)borates, and thus also synthesized $PhB(^{Ad}Im)_3NiNO$ (**2**).[77] The deprotonation of $[PhB(^{Ad}ImH)_3](OTf)_2$ with LDA occurs smoothly at room temperature and addition of $Ni(NO)Br(PPh_3)_2$ provides **2** as a maroon-red complex in 55% yield (Scheme 1C). Complex **2** was characterized by multinuclear NMR, SXRD, qNMR, and HRMS (see SI). A significantly downfield metal-bound carbene resonance is observed at δ 198.7 ppm in the $^{13}C\{^1H\}$ NMR spectrum (Figure S14). This carbene resonance is notably more downfield than that observed for **1**, a potential indicator that the donor strength of $PhB(^{Ad}Im)_3^-$ may be greater than that of $HB(^{CF3}mIm)_3^-$.[78] The SXRD structure of **2** is of high quality and confirms the presence of the $PhB(^{Ad}Im)_3^-$ ligand and the NO moiety, which has an N–O bond length of 1.183(4) Å (Figure 2). This bond length, as well as the Ni–N–O bond angle of 175.7(3)°, is comparable to that of other alkyl-substituted tris(imidazol-2-ylidene)borate $\{NiNO\}^{10}$ complexes.[60,73]

IR Spectroscopy of Complexes 1 and 2

We then assessed the donor strengths of $HB(^{CF3}mIm)_3^-$ and $PhB(^{Ad}Im)_3^-$, via the υ_{NO} of their respective complexes **1** and **2** with IR spectroscopy. The poor solubility of **1** in THF prevented direct comparison of its υ_{NO} to that of other reported $\{NiNO\}^{10}$ complexes of tris(carbene)borate ligands which are reported in THF solutions.[75] Despite this, we measured the υ_{NO} of **1** and **2** in both the solid state and in a THF-solvated film where a solid sample of the compound is treated with a few drops of THF and allowed to evaporate before recording the IR spectrum via an attenuated total reflectance (ATR) measurement. Using this method on **2** results in an identical υ_{NO} to the value measured in a THF solution within experimental error (Figure S25). We additionally wanted a benchmark to previously reported $\{NiNO\}^{10}$ scorpionate complexes.[75] To this end, we also prepared a sample of $PhB(^{tBu}Im)_3NiNO$ (**3**) in order to measure its υ_{NO} in the solid-state and as a THF-solvated film.[60]

The experimental solid state and THF-solvated film υ_{NO} data of **1**, **2**, and **3** are listed in Table 1. These values indicate that $PhB(^{Ad}Im)_3^-$ (υ_{NO} = 1693 cm^{-1}) and $PhB(^{tBu}Im)_3^-$ (υ_{NO} = 1695 cm^{-1}) are slightly stronger donors than $HB(^{CF3}mIm)_3^-$ (υ_{NO} = 1700 cm^{-1}) despite the highly-donating nature of the latter's mesoionic carbene donors. This is perhaps unsurprising due to the electron withdrawing nature of the trifluoromethyl substituents. However, we note that the donor strength of $HB(^{CF3}mIm)_3^-$ is commensurate to that of $PhB(^{Ad}Im)_3^-$ and $PhB(^{tBu}Im)_3^-$ as evidenced by the narrow 8 cm^{-1} range in their ν_{NO} values. Interestingly, $PhB(^{Ad}Im)_3^-$ is as donating as $PhB(^{CyCH2}Im)_3^-$ (υ_{NO} = 1693 cm^{-1}), which is the most donating alkyl-substituted tris(imidazol-2-ylidene)borate ligand reported in the literature to our knowledge.[75]

Computational Evaluation and Analysis of Ligand Donor Strengths

The experimental υ_{NO} values discussed above suggest that the electron withdrawing properties of the trifluoromethyl groups in **1** modulate the extremely strong donor properties that might be expected for the imidazol-5-ylidene donors. To explore this relationship, we performed DFT calculations to further understand the ligand donor properties of **1**, **2**, and **3**, as well as those of two theoretical complexes containing either *N*-trifluoromethylated imidazol-2-ylidene donors ($\mathbf{1}_{NHC}$) or methylated imidazol-5-ylidene carbene donors ($\mathbf{1}_{CH3}$). Geometry optimizations and frequency calculations were performed using the Gaussian 16 software package, with employment of the B3LYP functional, the 6-31G(d) basis set, and the Gaussian 16 default polarizable continuum

model (PCM) using the dielectric properties of THF.[81–84] A similar methodology was previously used for tris(carbene)borate-ligated {NiNO}^{10} complexes.[75] The calculated frequencies, listed in Table 1, agree with the experimental THF-film frequencies. Importantly, the calculated υ_{NO} for **1** is higher than that of **2** and **3**, but still comparable in magnitude, in agreement with the experimental results.

We used these experimentally calibrated DFT calculations to estimate the υ_{NO} of the hypothetical complexes $\mathbf{1}_{NHC}$ and $\mathbf{1}_{CH3}$ (see structures in Table 1). We hypothesized that $\mathbf{1}_{NHC}$, which differs from **1** by having imidazol-2-ylidene rather than imidazol-5-ylidene donors, would have the largest υ_{NO} and weakest donation due the presence of electron withdrawing *N*-trifluoromethyl substituents and the comparatively weaker sigma donation of imidazol-2-ylidenes compared to mesoionic imidazol-5-ylidenes. Conversely, we hypothesized that $\mathbf{1}_{CH3}$, the non-fluorinated congener of **1**, would have the lowest υ_{NO}. Indeed, the calculated υ_{NO} of $\mathbf{1}_{NHC}$ and $\mathbf{1}_{CH3}$ are the highest and lowest of the examined set. We note that the predicted υ_{NO} of $\mathbf{1}_{NHC}$ is ~50 cm^{-1} higher (weaker) than the next closest analogue (**1**), supporting the importance of using imidazol-5-ylidene motifs to preserve good donor properties. Overall, these frequency calculations support our experimental findings that the additional electron donation from imidazol-5-ylidene arms is balanced out by the incorporation of trifluoromethyl groups.

We then performed an NBO analysis to examine if the donor properties of HB(^{CF3}mIm)$_3^-$ arise from inductive weakening of σ-donation, or if the trifluoromethyl substituents engender significant metal-ligand π-backbonding. Specifically, we conducted a second order perturbative energy analysis on each of the optimized structures of the complexes in Table 1. The analyses were carried out using the NBO6 program included with the Gaussian 09 package.[85,86] The analyses allow us to estimate the strength of localized, secondary bonding interactions between the carbene donors and the NiNO center. Particularly, we examined the energies of interaction between filled NBOs representative of the carbene lone pair σ-donors and nonbonding and antibonding orbitals of the NiNO fragment, and between filled Ni-centered *d*-orbitals and the π* orbital located on the carbene carbon ($\pi^*_{C:}$, see SI). This approach is based on a previous investigation evaluating backbonding in transition metal–NHC complexes.[87] The ligand arm-averaged summed energies of both carbene-to-NiNO σ-donation interactions and Ni-to-$\pi^*_{C:}$ π-backdonation interactions for all five complexes are listed in Table 1.

As expected, we observe a negative correlation between σ-donation interaction energy and both the experimental and

Table 1. Experimental and theoretical ν_{NO} values and NBO second-order perturbative bonding interaction energies of selected {NiNO}^{10} complexes. Note that a scaling factor of 0.9614 was applied to each calculated stretching frequency.

Cmpd	Structure	Experimental υ_{NO} (cm^{-1})		Calculated υ_{NO} (cm^{-1})	L→M σ-bonding per arm (kcal/mol)	L→M π-backbonding per arm (kcal/mol)
		solid state	THF film	THF		
$\mathbf{1}_{NHC}$	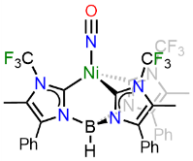	—	—	1764	53.6	9.5
1	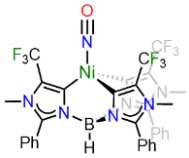	1695	1700	1712	71.5	7.6
3	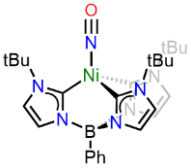	1692	1695	1698	76.0	8.3
2	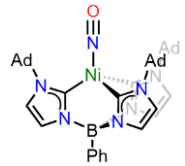	1689	1693	1697	97.9	8.0
$\mathbf{1}_{CH3}$	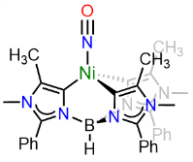	—	—	1637	105.8	9.4

calculated ν_{NO}. Of the complexes featuring imidazol-2-ylidene donors, $\mathbf{1}_{NHC}$ has the lowest σ-donation interaction energy. This supports the previously reported finding that changing the *N*-bound alkyl or aryl substituent on the tris(imidazol-2-ylidene)borate framework has significant effects on overall ligand donor strength.[75] Conversely, we note the very large σ-donation interaction energy calculated for $\mathbf{1}_{CH3}$, which is almost 8 kcal/mol greater than that calculated for **2** and more than 30 kcal/mol greater than that calculated for **1**. This result coheres with prior reports that imidazol-5-ylidene donors are much better σ-donors than imidazol-2-ylidene donors.[72,73] Furthermore, this result demonstrates how the trifluoromethyl groups weaken the donor strength of the mesoionic imidazol-5-ylidene donors. The π-back-donation interaction energies for all the analyzed complexes generally do not exhibit any meaningful correlation to experimental or calculated ν_{NO}, suggesting that the observed differences in donor strength primarily arise from inductive changes to σ-donation.

Conclusions

We have designed, synthesized, and metalated the first example of a tris(imidazol-5-ylidene)borate ligand. Furthermore, this ligand scaffold features an oxidatively robust, fluorinated coordination pocket. The preparation of its {NiNO}^{10} complex, as well as that of the PhB(^{Ad}Im)$_3^-$ ligand, allows evaluation of relative ligand donor strengths via comparison of ν_{NO} values. The relative ligand donor strengths were also computationally explored with DFT calculations and NBO analysis. These analyses reveal that the incorporation of electron-withdrawing trifluoromethyl groups results in a tris(imidazol-5-ylidene)borate ligand with modulated donation on par with previously reported alkyl substituted imidazol-2-ylidene-based scaffolds. This observation, coupled with the marked success of tris(imidazol-2-ylidene)borate ligands in the stabilization and isolation of high-valent complexes featuring metal-ligand multiple bonds, suggests that this new fluorinated ligand scaffold holds promise for the support and isolation of highly reactive intermediates that might otherwise oxidatively decompose.

Experimental Section

General Considerations.

All manipulations were performed under a dry nitrogen atmosphere using either standard Schlenk techniques or in an mBraun Unilab Pro glovebox unless otherwise stated. All chemicals were obtained from commercial sources and used as received unless otherwise stated. Solvents were dried on a solvent purification system from Pure Process Technologies before storing over 4 Å molecular sieves under N_2. Tetrahydrofuran (THF) and diethyl ether (Et_2O) were stirred over NaK alloy and passed through a column of activated alumina prior to storing over 4 Å sieves under N_2. Ni(NO)Br(PPh_3)$_2$, [PhB(^{Ad}ImH)$_3$](OTf)$_2$, [PhB(^{tBu}ImH)$_3$](OTf)$_2$, and PhB(^{tBu}Im)$_3$NiNO (**3**) were prepared according to previously reported procedures.[49,60,77,88] ^{1}H, ^{11}B{^{1}H}, ^{13}C{1H}, and ^{19}F{^{1}H} NMR spectra were recorded on either a 400 MHz Bruker DRX spectrometer equipped with a BBO probe or a 500 MHz Bruker Avance-III-HD spectrometer equipped with a BBFO SmartProbe. ^{1}H and ^{13}C{^{1}H} spectra were referenced to residual proteo-solvent peaks.[89] ^{11}B{^{1}H} spectra were baseline corrected to remove the signal from the borosilicate tube. IR spectra were recorded on either a Bruker Tensor II spectrometer with the OPUS software suite as THF solutions in a KBr-walled solution cell or a Bruker Alpha II spectrometer in a glovebox with the OPUS software suite as solids or THF-solvated films on a Platinum Diamond ATR module. Combustion analysis was performed by Midwest Microlabs. High-resolution mass spectra were collected on an Agilent 6224 Accurate-Mass TOF GC/MS installed with an ESI/APCI ion source.

Both complexes **1** and **2** provided relatively poor combustion analysis. As such, we assayed the bulk purity of **2** with qNMR rather than combustion analysis.[90–94] A 1,3,5-trimethoxybenzene (TMB) standard (58.5 μmol) was added to solution of **2** in CD_2Cl_2. A single-scan ^{1}H NMR spectrum was then collected. The relative peak integrations of TMB (δ_{TMB} = 6.06 and 3.75 ppm) and each compound proton were recorded and used to determine the percent purity with the formula below (*n* = number of protons giving rise to the integral, *int* = integral value, *MW* = molecular weight, *m* = exact weight of sample). The value reported for **2** represents an average of the percent purity as determined for each ligand proton signal relative to both standard signals.

$$P\,[\%] = \frac{n_{TMB} * int_{\mathbf{2}} * MW_{\mathbf{2}} * m_{TMB}}{n_{\mathbf{2}} * int_{TMB} * MW_{TMB} * m_{\mathbf{2}}}$$

Computational Details.

N–O stretching frequency determination and second-order perturbation energy analysis procedures were adapted from literature reports.[75,87] Geometry optimizations and frequency calculations were performed in Gaussian16, Revision A.03 using the B3LYP functional, the 6-31G(d) basis set, and the Gaussian default polarizable continuum model with the dielectric constant of THF.[81–84] Frequency calculations were performed analytically. All minima were confirmed to have zero imaginary frequencies. A scaling factor of 0.9614 was applied to each calculated stretching frequency reported above. Second-order perturbative NBO analysis was carried out using the NBO6 program included in Gaussian 09, Revision D.01. The analyses were carried out on the Gaussian 16 optimized geometries from above, also using the B3LYP functional and 6-31G(d) basis set. Additional computational detail regarding the NBO analysis can be found in the Supporting Information.

Crystallographic Details.

The diffraction data for **1** were measured at 100 K on a XtalAB Synergy-*S* Dual Source Single Crystal X-ray Diffractometer using PhotonJet-S Cu 50W Microfocus X-ray source (λ = 1.54184 Å) and HyPix-6000HE Hybrid Photon Counting detector. The diffraction data for **2** were measured at 100 K on a XtalAB Synergy-*S* Dual Source Single Crystal X-ray Diffractometer using PhotonJet-S Mo 50W Microfocus X-ray source (λ = 0.71073 Å) and HyPix-6000HE Hybrid Photon Counting detector.

Data reduction and integration for both **1** and **2** were performed with the CrysAlisPro 1.171.43.75a (Rigaku Oxford Diffraction, 2023) software package, with numerical absorption correction based on Gaussian integration over a multifaceted crystal model and empirical absorption correction using spherical harmonics, implemented in SCALE3 ABSPACK scaling algorithm. The structures were solved by SHELXT (Version 2018/2)[95] and refined by a full-matrix least-squares procedure using OLEX2 (XL refinement program version 2018/3).[96,97]

The precision of the X-ray analysis of **1** is limited due to the weak crystal diffraction from heavy molecular disorder within the crystal. We note that this was the best diffracting sample out of numerous crystallization attempts. The disorder was possible to model, and the structure refinement was performed with the use of geometric and displacement ellipsoids restraints and constraints. Nevertheless, the results are of sufficient quality for connectivity comparison between **1** and **2** and do not affect the general discussion of the complexes. Additional crystallographic and refinement data can be found in the Supporting Information.

Synthesis of 1-methyl-2-phenyl-1H-imidazole.

A 1 L round bottom flask was charged with 2-phenylimidazole (30 g, 210 mmol) and 600 mL of acetonitrile. The mixture was cooled in an ice bath to 0 °C and stirred. NaH, as a 60% dispersion in mineral oil (9.2 g, 230 mmol), was washed with hexanes and then carefully added to the reaction mixture. After all the hydride was incorporated and bubbling had ceased then a solution of methyl iodide (14.3 mL, 230 mmol) in 150 mL acetonitrile was added dropwise. The reaction was stirred for 3 h and then concentrated via rotary evaporation. The resulting crude product was washed with aqueous NaOH (~1 M) and extracted three times with diethyl ether. The combined organic layers were passed through an alumina plug, washed with brine, dried with a copious amount of anhydrous magnesium sulfate, and filtered through alumina. The solution was dried to a yellow solid (23 g, 70% yield) which was used without further purification. The spectral data for this compound matches a previous literature report.[98] ^{1}H NMR ($CDCl_3$, 400 MHz): δ 7.63 (2H, Ph-*H*), 7.44 (3H, Ph-*H*), 7.13 (1H, Imid-*H*), 6.97 (Imid-*H*), 3.75 (3H, Me-*H*).

Synthesis of 5-trifluoromethyl-1-methyl-2-phenyl-1H-imidazole.

This procedure was modified from a literature procedure.[76] A 1 L Schlenk flask was charged with 1-methyl-2-phenyl-1H-imidazole (12 g, 76 mmol), (diacetoxyiodo)benzene (49 g, 150 mmol), cesium fluoride (35 g, 230 mmol), and 600 mL acetonitrile. The mixture was heated to 70 °C and stirred. A solution of (trimethylsilyl)trifluoromethane (32 g, 230 mmol) in 100 mL acetonitrile was added dropwise. The reaction was allowed to cool to room temperature and stirred overnight. Acetonitrile was removed by rotary evaporation and the resulting crude product was washed with saturated sodium bicarbonate and extracted three times with dichloromethane. The combined organic layers were washed with water, dried with anhydrous magnesium sulfate, and filtered through alumina. Dichloromethane was removed by rotary evaporation and the crude material was purified by column chromatography (500 mL of alumina, 15% ethyl acetate in hexanes). Fractions with large amounts of impurities were discarded and the remaining eluent was removed by rotary evaporation. The resulting crude product was recrystallized from 15% ethyl acetate in hexanes to obtain off-white crystals (5.1 g, 30% yield). The spectral data for this compound matches a previous literature report.[99] ^{1}H NMR ($CDCl_3$, 400 MHz): δ 7.62 (2H, Ph-*H*), 7.52 (4H, Ph-*H* and Imid-*H*), 3.78 (3H, Me-*H*).

Synthesis of [HB(^{CF3}mImH)$_3$](OTf)$_2$.

This procedure was based on literature procedures.[73] A 1 L Schlenk flask was charged with 5-trifluoromethyl-1-methyl-2-phenyl-1*H*-imidazole (8.1 g, 36 mmol) and 200 mL of toluene. While stirring, dibromoborane dimethylsulfide as a 1.0 M solution in dichloromethane (11 mL, 11 mmol) was added, resulting in a cloudy solution. This solution was heated to 100 °C, which clarified the solution, and trimethylsilyl trifluoromethanesulfonate (5.5 mL, 25 mmol) was added. The reaction was stirred for two nights at 100 °C. The precipitate was filtered off and washed with diethyl ether, then hot 1,2-dichloroethane, and then diethyl ether again. The resulting white powder (8 g, 60% yield) was dried on a high vacuum line until no dichloroethane was visible by ^{1}H NMR spectroscopy and characterized and used without further purification. ^{1}H NMR (CD_3CN, 400 MHz): δ 7.86 (3H, Imid–*H*), δ 7.60 (3H, Ph-*H*), 7.42 (6H, Ph-*H*), 6.86 (6H, Ph-*H*), 3.62 (9H, Me-*H*). We do not observe a signal from the B–*H* proton by ^{1}H NMR spectroscopy. ^{13}C{^{1}H} NMR (CD_3CN, 500 MHz): δ 151.7, 132.6, 129.7, 129.3, 125.1 (q, J = 4.2 Hz), 124.4 (q, J = 42.1 Hz), 121.5 (q, J = 268 Hz), 34.4 (q, J = 1.8 Hz). ^{11}B{^{1}H} NMR (CD_3CN, 400 MHz): δ -5.0 ^{19}F{^{1}H} NMR (CD_3CN, 400 MHz): δ -61.9 , -79.3. IR (solid, cm^{-1}): 2610, 2550 (w, B–H). Anal. calcd for $C_{35}H_{28}BF_{15}N_6O_6S_2$: C 42.53, H 2.86, N 8.50. Found: C 42.29, H 2.88, N 8.43.

*Synthesis of HB(^{CF3}mIm)$_3$NiNO (**1**).*

A solution of LiHMDS (87.5 mg, 0.52 mmol) in THF (2 mL) cooled to −55°C was added to a stirred slurry of [HB(^{CF3}*m*ImH)$_3$](OTf)$_2$ (204.7 mg, 0.207 mmol) in THF (8 mL) cooled to −55°C. The reaction was stirred at temperature for 1 h to yield a translucent, light orange solution. At this point, the reaction was transferred to a chilled vial containing Ni(NO)(Br)(PPh_3)$_2$ (143.8 mg, 0.207 mmol), and then stirred at ambient temperature for 4 h. The reaction was then cooled back down to −55°C, at which point a solution of LiHMDS (52.5 mg, 0.31 mmol) in THF (2 mL) cooled to −55°C was added to the reaction. The reaction was then allowed to stir at ambient temperature for 16 h. The reaction mixture was then concentrated to ~2 mL, chilled to −35°C, and then filtered through a fine-fritted Buchner funnel. The collected material was washed with ~ 15 mL of THF and dried to give a red-orange solid (32 mg, 20% yield). Crystals suitable for X-ray diffraction were grown from diffusion of *n*-pentane to a dichloromethane solution of the complex at ambient temperature. ^{1}H NMR (CD_3CN, 500 MHz): δ 7.35 (3H, Ph-*H*), 7.12 (6H, Ph-*H*), 6.93 (6H, Ph-*H*), 3.51 (9H, Me-*H*). We do not observe a signal from the B–*H* proton by

^{1}H NMR spectroscopy. ^{13}C{^{1}H} (DMF-d_7, 500 MHz): δ 180.2, 150.9, 130.5, 130.3, 129.0 (q, J = 35 Hz), 128.1, 125.4, 124.1 (q, J = 265 Hz), 32.8 (q, J = 2 Hz). ^{11}B{^{1}H} NMR (DMF-d_7, 500 MHz): δ -8.03. ^{19}F{^{1}H} (DMF-d_7, 500 MHz); δ 56.8. IR: (solid, cm^{-1}) 2573, 2562 (w, B–H), 1695 (s, N–O); (THF-solvated film, cm^{-1}) 2570, 2554 (w, B–H), 1700 (s, N–O). HRMS (ESI) *m/z*: [M]$^{+}$ calcd for $C_{33}H_{25}BN_7F_9NiO$: 774.1460; found, 774.1432. The poor solubility of this compound precluded characterization by qNMR, but NMR spectroscopy supports the bulk purity of this complex (see SI).

*Synthesis of PhB(^{Ad}Im)$_3$NiNO (**2**).*
A solution of LDA (59 mg, 0.547 mmol) dissolved in THF (2 mL) was added to a stirred slurry of PhB(^{Ad}ImH)$_3$OTf$_2$ (175 mg, 0.177 mmol) in THF (8 mL). The reaction was stirred at ambient temperature for 1 h. At this point, the reaction was transferred to a vial containing Ni(NO)(Br)(PPh$_3$)$_2$ (122 mg, 0.177 mmol), and the resulting solution was stirred for 16 hours. The solution was pumped down and triterated with pentane and then extracted with toluene and filtered through Celite. The filtrate was dried under vacuum and triterated with pentane. This solid was then washed with ~10 mL of MeCN, dried, and then extracted with DCM and filtered through Celite. Drying under vacuum yielded a deep red solid (77.0 mg, 55% yield). Crystals suitable for X-ray diffraction were grown from diffusion of *n*-pentane to a THF solution of the complex at ambient temperature. ^{1}H NMR (C_6D_6, 400 MHz): δ 8.05 (2H, Ph-*H*), 7.39 (2H, Ph-*H*), 7.35 (1H, Ph-*H*), 7.04 (3H, Im-*H*), 6.79 (3H, Im-*H*), 2.54 (18H, Ad-*H*), 2.09 (9H, Ad-*H*), 1.70 (18H, Ad-*H*). ^{13}C{^{1}H} (C_6D_6, 400 MHz): δ 198.7, 135.5, 128.2, 127.9, 127.4, 122.1, 116.3, 57.4, 43.0, 36.3, 30.5. ^{11}B{^{1}H} NMR (C_6D_6, 400 MHz): δ -1.63. IR: (solid, cm^{-1}) 1689 (s, N–O); (THF, cm^{-1}) 1692 (s, N–O); (THF-solvated film, cm^{-1}) 1693 cm^{-1} (s, N–O). qNMR (^{1}H NMR, CD_2Cl_2, 500MHz, with 1,3,5-trimethoxybenzene standard): 96%. HRMS (ESI) *m/z*: [M]$^{+}$ calcd for $C_{45}H_{56}BN_7NiO$: 778.4029; found, 778.4073.

Associated Content

Supporting Information.

NMR and IR spectra, X-ray crystallographic data collection and refinement parameters for **1** and **2**, DFT calculation details, and DFT optimized structures in XYZ format data. This material is available free of charge via the Internet at http://pubs.acs.org.

Accession Codes

CCDC 2294049-2294050 contains the supplementary crystallographic data for this paper. These data can be obtained free of charge via www.ccdc.cam.ac.uk/data_request/cif, or by emailing data_request@ccdc.cam.ac.uk, or by contacting The Cambridge Crystallographic Data Centre, 12 Union Road, Cambridge CB2 1EZ, UK; fax: +44 1223 336033.

Author Information

Corresponding Author

*John S. Anderson. Email: jsanderson@uchicago.edu.

Author Contributions

The manuscript was written through contributions of all authors. Joseph S. Scott and Joseph E. Schneider contributed equally to the manuscript. All authors have given approval to the final version of the manuscript.

Notes

The authors declare no competing financial interest.

Acknowledgements

This work was funded by the National Institutes of Health (R35 GM133470), the National Science Foundation (1654144), and the University of Chicago. Computations were generously supported by the UChicago Research Computing Center. J.E.S. thanks the Department of Defense for a National Defense and Engineering Graduate Fellowship (00003765), and J.S.A. the Dreyfus Foundation for a Teacher-Scholar award (TC-21-064). This work made use of the IMSERC Crystallography facility at Northwestern University, which has received support from the Soft and Hybrid Nanotechnology Experimental (SHyNE) Resource (NSF ECCS-2025633), and Northwestern University. We would also like to thank Charlotte Stern and Christos D. Malliakas for their assistance with SXRD acquisition at IMSERC.

References

(1) Schrock, R. R. Catalytic Reduction of Dinitrogen to Ammonia at a Single Molybdenum Center. *Acc. Chem. Res.* **2005**, *38* (12), 955–962. https://doi.org/10.1021/ar0501121.

(2) Mehn, M. P.; Peters, J. C. Mid- to High-Valent Imido and Nitrido Complexes of Iron. *J. Inorg. Biochem.* **2006**, *100* (4), 634–643. https://doi.org/10.1016/j.jinorgbio.2006.01.023.

(3) Rittle, J.; Green, M. T. Cytochrome P450 Compound I: Capture, Characterization, and C-H Bond Activation Kinetics. *Science* **2010**, *330* (6006), 933–937. https://doi.org/10.1126/science.1193478.

(4) Crossland, J. L.; Tyler, D. R. Iron–Dinitrogen Coordination Chemistry: Dinitrogen Activation and Reactivity. *Coord. Chem. Rev.* **2010**, *254* (17–18), 1883–1894. https://doi.org/10.1016/j.ccr.2010.01.005.

(5) Itoh, S. Developing Mononuclear Copper–Active-Oxygen Complexes Relevant to Reactive Intermediates of Biological Oxidation Reactions. *Acc. Chem. Res.* **2015**, *48* (7), 2066–2074. https://doi.org/10.1021/acs.accounts.5b00140.

(6) Guo, M.; Corona, T.; Ray, K.; Nam, W. Heme and Nonheme High-Valent Iron and Manganese Oxo Cores in Biological and Abiological Oxidation Reactions. *ACS Cent. Sci.* **2019**, *5* (1), 13–28. https://doi.org/10.1021/acscentsci.8b00698.

(7) Collman, J. P.; Zhang, X.; Lee, V. J.; Uffelman, E. S. Reg Oselective and Enantioselective Epoxidation Catalyzed by Metalloporphyrins. **1993**, *261*.

(8) Davies, H. M. L.; Hansen, T.; Churchill, M. R. Catalytic Asymmetric C−H Activation of Alkanes and

Tetrahydrofuran. *J. Am. Chem. Soc.* **2000**, *122* (13), 3063–3070. https://doi.org/10.1021/ja994136c.

(9) Müller, P.; Fruit, C. Enantioselective Catalytic Aziridinations and Asymmetric Nitrene Insertions into CH Bonds. *Chem. Rev.* **2003**, *103* (8), 2905–2920. https://doi.org/10.1021/cr020043t.

(10) Scott, J.; Basuli, F.; Fout, A. R.; Huffman, J. C.; Mindiola, D. J. Evidence for the Existence of a Terminal Imidoscandium Compound: Intermolecular C□H Activation and Complexation Reactions with the Transient Sc□NAr Species. *Angew. Chem. Int. Ed.* **2008**, *47* (44), 8502–8505. https://doi.org/10.1002/anie.200803325.

(11) Borovik, A. S. Role of Metal–Oxo Complexes in the Cleavage of C–H Bonds. *Chem. Soc. Rev.* **2011**, *40* (4), 1870. https://doi.org/10.1039/c0cs00165a.

(12) Hashiguchi, B. G.; Bischof, S. M.; Konnick, M. M.; Periana, R. A. Designing Catalysts for Functionalization of Unactivated C–H Bonds Based on the CH Activation Reaction. *Acc. Chem. Res.* **2012**, *45* (6), 885–898. https://doi.org/10.1021/ar200250r.

(13) Camasso, N. M.; Sanford, M. S. Design, Synthesis, and Carbon-Heteroatom Coupling Reactions of Organometallic Nickel(IV) Complexes. *Science* **2015**, *347* (6227), 1218–1220. https://doi.org/10.1126/science.aaa4526.

(14) Collins, T. J.; Ryabov, A. D. Targeting of High-Valent Iron-TAML Activators at Hydrocarbons and Beyond. *Chem. Rev.* **2017**, *117* (13), 9140–9162. https://doi.org/10.1021/acs.chemrev.7b00034.

(15) Wu, P.; Yap, G. P. A.; Theopold, K. H. Synthesis, Characterization, and Reactivity of Chromium(VI) Alkylidenes. *Organometallics* **2019**, *38* (24), 4593–4600. https://doi.org/10.1021/acs.organomet.9b00604.

(16) Kal, S.; Xu, S.; Que, L. Bio-inspired Nonheme Iron Oxidation Catalysis: Involvement of Oxoiron(V) Oxidants in Cleaving Strong C−H Bonds. *Angew. Chem. Int. Ed.* **2020**, *59* (19), 7332–7349. https://doi.org/10.1002/anie.201906551.

(17) Zhang, L.; Mathew, S.; Hessels, J.; Reek, J. N. H.; Yu, F. Homogeneous Catalysts Based on First-Row Transition-Metals for Electrochemical Water Oxidation. *ChemSusChem* **2021**, *14* (1), 234–250. https://doi.org/10.1002/cssc.202001876.

(18) Kondo, M.; Tatewaki, H.; Masaoka, S. Design of Molecular Water Oxidation Catalysts with Earth-Abundant Metal Ions. *Chem. Soc. Rev.* **2021**, *50* (12), 6790–6831. https://doi.org/10.1039/D0CS01442G.

(19) Kanan, M. W.; Nocera, D. G. In Situ Formation of an Oxygen-Evolving Catalyst in Neutral Water Containing Phosphate and Co^{2+}. *Science* **2008**, *321* (5892), 1072–1075. https://doi.org/10.1126/science.1162018.

(20) Betley, T. A.; Wu, Q.; Van Voorhis, T.; Nocera, D. G. Electronic Design Criteria for O−O Bond Formation via Metal−Oxo Complexes. *Inorg. Chem.* **2008**, *47* (6), 1849–1861. https://doi.org/10.1021/ic701972n.

(21) Concepcion, J. J.; Jurss, J. W.; Brennaman, M. K.; Hoertz, P. G.; Patrocinio, A. O. T.; Murakami Iha, N. Y.; Templeton, J. L.; Meyer, T. J. Making Oxygen with Ruthenium Complexes. *Acc. Chem. Res.* **2009**, *42* (12), 1954–1965. https://doi.org/10.1021/ar9001526.

(22) Das, D.; Pattanayak, S.; Singh, K. K.; Garai, B.; Sen Gupta, S. Electrocatalytic Water Oxidation by a Molecular Cobalt Complex through a High Valent Cobalt Oxo Intermediate. *Chem. Commun.* **2016**, *52* (79), 11787–11790. https://doi.org/10.1039/C6CC05773J.

(23) Nguyen, A. I.; Wang, J.; Levine, D. S.; Ziegler, M. S.; Tilley, T. D. Synthetic Control and Empirical Prediction of Redox Potentials for Co_4O_4 Cubanes over a 1.4 V Range: Implications for Catalyst Design and Evaluation of High-Valent Intermediates in Water Oxidation. *Chem. Sci.* **2017**, *8* (6), 4274–4284. https://doi.org/10.1039/C7SC00627F.

(24) Collins, T. J. Designing Ligands for Oxidizing Complexes. *Acc. Chem. Res.* **1994**, *27* (9), 279–285. https://doi.org/10.1021/ar00045a004.

(25) Thorarinsdottir, A. E.; Nocera, D. G. Energy Catalysis Needs Ligands with High Oxidative Stability. *Chem Catal.* **2021**, *1* (1), 32–43. https://doi.org/10.1016/j.checat.2021.05.012.

(26) Gil-Sepulcre, M.; Llobet, A. Molecular Water Oxidation Catalysts Based on First-Row Transition Metal Complexes. *Nat. Catal.* **2022**, *5* (2), 79–82. https://doi.org/10.1038/s41929-022-00750-1.

(27) Renz, M.; Hemmert, C. Isolation and Characterization of an Oxidative Degradation Product of a Polypyridine Ligand. *Chem. Commun.* **1998**, No. 16, 1635–1636. https://doi.org/10.1039/a803255f.

(28) Yokota, S.; Tachi, Y.; Itoh, S. Oxidative Degradation of β -Diketiminate Ligand in Copper(II) and Zinc(II) Complexes. *Inorg. Chem.* **2002**, *41* (6), 1342–1344. https://doi.org/10.1021/ic0156238.

(29) Hu, X.; Meyer, K. Terminal Cobalt(III) Imido Complexes Supported by Tris(Carbene) Ligands: Imido Insertion into the Cobalt−Carbene Bond. *J. Am. Chem. Soc.* **2004**, *126* (50), 16322–16323. https://doi.org/10.1021/ja044271b.

(30) Sander, A. C.; Schober, A.; Dechert, S.; Meyer, F. A Pyrazolate-Bridged Bis(Pentadentate) Ligand and Its Dinuclear Ruthenium Complex. *Eur. J. Inorg. Chem.* **2015**, *2015* (26), 4348–4353. https://doi.org/10.1002/ejic.201500469.

(31) Keilwerth, M.; Hohenberger, J.; Heinemann, F. W.; Sutter, J.; Scheurer, A.; Fang, H.; Bill, E.; Neese, F.; Ye, S.; Meyer, K. A Series of Iron Nitrosyl Complexes $\{Fe–NO\}^{6–9}$ and a Fleeting $\{Fe–NO\}^{10}$ Intermediate En Route to a Metalacyclic Iron Nitrosoalkane. *J. Am. Chem. Soc.* **2019**, *141* (43), 17217–17235. https://doi.org/10.1021/jacs.9b08053.

(32) Keilwerth, M.; Grunwald, L.; Mao, W.; Heinemann, F. W.; Sutter, J.; Bill, E.; Meyer, K. Ligand Tailoring Toward an Air-Stable Iron(V) Nitrido Complex. *J. Am. Chem. Soc.* **2021**, *143* (3), 1458–1465. https://doi.org/10.1021/jacs.0c11141.

(33) Mao, W.; Zhang, Z.; Fehn, D.; Jannuzzi, S. A. V.; Heinemann, F. W.; Scheurer, A.; Van Gastel, M.; DeBeer, S.; Munz, D.; Meyer, K. Synthesis and Reactivity of a Cobalt-Supported Singlet Nitrene. *J. Am.*

Chem. Soc. **2023**, *145* (25), 13650–13662. https://doi.org/10.1021/jacs.3c01478.

(34) Reinaud, O. M.; Theopold, K. H. Hydrogen Tunneling in the Activation of Dioxygen by a Tris(Pyrazolyl)Borate Cobalt Complex. *J. Am. Chem. Soc.* **1994**, *116* (15), 6979–6980. https://doi.org/10.1021/ja00094a080.

(35) Thyagarajan, S.; Incarvito, C. D.; Rheingold, A. L.; Theopold, K. H. Formation and Reactivity of a Cobalt(II) Hydroperoxide Intermediate. *Chem. Commun.* **2001**, No. 21, 2198–2199. https://doi.org/10.1039/b107080k.

(36) Hikichi, S.; Yoshizawa, M.; Sasakura, Y.; Komatsuzaki, H.; Moro-oka, Y.; Akita, M. Structural Characterization and Intramolecular Aliphatic C−H Oxidation Ability of MIII(μ-O)2MIII Complexes of Ni and Co with the Hydrotris(3,5-Dialkyl-4-X-Pyrazolyl)Borate Ligands TpMe2,X (X=Me, H, Br) and TpiPr2. *Chem. - Eur. J.* **2001**, *7* (23), 5011–5028. https://doi.org/10.1002/1521-3765(20011203)7:23<5011::AID-CHEM5011>3.0.CO;2-C.

(37) Jensen, M. P.; Mehn, M. P.; Que, L. Intramolecular Aromatic Amination through Iron-Mediated Nitrene Transfer. *Angew. Chem. Int. Ed.* **2003**, *42* (36), 4357–4360. https://doi.org/10.1002/anie.200351605.

(38) Thyagarajan, S.; Shay, D. T.; Incarvito, C. D.; Rheingold, A. L.; Theopold, K. H. Intramolecular C−H Activation by Inferred Terminal Cobalt Imido Intermediates. *J. Am. Chem. Soc.* **2003**, *125* (15), 4440–4441. https://doi.org/10.1021/ja028267g.

(39) Shay, D. T.; Yap, G. P. A.; Zakharov, L. N.; Rheingold, A. L.; Theopold, K. H. Intramolecular C?H Activation by an Open-Shell Cobalt(III) Imido Complex. *Angew. Chem. Int. Ed.* **2005**, *44* (10), 1508–1510. https://doi.org/10.1002/anie.200462529.

(40) Eckert, N. A.; Vaddadi, S.; Stoian, S.; Lachicotte, R. J.; Cundari, T. R.; Holland, P. L. Coordination-Number Dependence of Reactivity in an Imidoiron(III) Complex. *Angew. Chem. Int. Ed.* **2006**, *45* (41), 6868–6871. https://doi.org/10.1002/anie.200601927.

(41) King, E. R.; Sazama, G. T.; Betley, T. A. Co(III) Imidos Exhibiting Spin Crossover and C–H Bond Activation. *J. Am. Chem. Soc.* **2012**, *134* (43), 17858–17861. https://doi.org/10.1021/ja307699u.

(42) Zhang, L.; Liu, Y.; Deng, L. Three-Coordinate Cobalt(IV) and Cobalt(V) Imido Complexes with N-Heterocyclic Carbene Ligation: Synthesis, Structure, and Their Distinct Reactivity in C–H Bond Amination. *J. Am. Chem. Soc.* **2014**, *136* (44), 15525–15528. https://doi.org/10.1021/ja509731z.

(43) Du, J.; Wang, L.; Xie, M.; Deng, L. A Two-Coordinate Cobalt(II) Imido Complex with NHC Ligation: Synthesis, Structure, and Reactivity. *Angew. Chem. Int. Ed.* **2015**, *54* (43), 12640–12644. https://doi.org/10.1002/anie.201505937.

(44) Cheng, J.; Liu, J.; Leng, X.; Lohmiller, T.; Schnegg, A.; Bill, E.; Ye, S.; Deng, L. A Two-Coordinate Iron(II) Imido Complex with NHC Ligation: Synthesis, Characterization, and Its Diversified Reactivity of Nitrene Transfer and C–H Bond Activation. *Inorg. Chem.* **2019**, *58* (11), 7634–7644. https://doi.org/10.1021/acs.inorgchem.9b01147.

(45) Goetz, M. K.; Schneider, J. E.; Filatov, A. S.; Jesse, K. A.; Anderson, J. S. Enzyme-Like Hydroxylation of Aliphatic C–H Bonds From an Isolable Co-Oxo Complex. *J. Am. Chem. Soc.* **2021**, *143* (49), 20849–20862. https://doi.org/10.1021/jacs.1c09280.

(46) Rogers, M.; Stahl, S. N-Heterocyclic Carbenes as Ligands for High-Oxidation-State Metal Complexes and Oxidation Catalysis. *N-Heterocycl. Carbenes Transit. Met. Catal.* **2007**, 21–46.

(47) Saouma, C. T.; Peters, J. C. ME and ME Complexes of Iron and Cobalt That Emphasize Three-Fold Symmetry (E=O, N, NR). *Coord. Chem. Rev.* **2011**, *255* (7–8), 920–937. https://doi.org/10.1016/j.ccr.2011.01.009.

(48) Nieto, I.; Cervantes-Lee, F.; Smith, J. M. A New Synthetic Route to Bulky “Second Generation” Tris(Imidazol-2-Ylidene)Borate Ligands: Synthesis of a Four Coordinate Iron(Ii) Complex. *Chem. Commun.* **2005**, No. 30, 3811. https://doi.org/10.1039/b505985b.

(49) Cowley, R. E.; Bontchev, R. P.; Duesler, E. N.; Smith, J. M. Removing the Sting from the Tail: Reversible Protonation of Scorpionate Ligands in Cobalt(II) Tris(Carbene)Borate Complexes. *Inorg. Chem.* **2006**, *45* (24), 9771–9779. https://doi.org/10.1021/ic061299a.

(50) Nieto, I.; Ding, F.; Bontchev, R. P.; Wang, H.; Smith, J. M. Thermodynamics of Hydrogen Atom Transfer to a High-Valent Iron Imido Complex. *J. Am. Chem. Soc.* **2008**, *130* (9), 2716–2717. https://doi.org/10.1021/ja0776834.

(51) Vogel, C.; Heinemann, F. W.; Sutter, J.; Anthon, C.; Meyer, K. An Iron Nitride Complex. *Angew. Chem.* **2008**, *120* (14), 2721–2724. https://doi.org/10.1002/ange.200800600.

(52) Scepaniak, J. J.; Vogel, C. S.; Khusniyarov, M. M.; Heinemann, F. W.; Meyer, K.; Smith, J. M. Synthesis, Structure, and Reactivity of an Iron(V) Nitride. *Science* **2011**, *331* (6020), 1049–1052. https://doi.org/10.1126/science.1198315.

(53) Ding, M.; Cutsail Iii, G. E.; Aravena, D.; Amoza, M.; Rouzières, M.; Dechambenoit, P.; Losovyj, Y.; Pink, M.; Ruiz, E.; Clérac, R.; Smith, J. M. A Low Spin Manganese(IV) Nitride Single Molecule Magnet. *Chem. Sci.* **2016**, *7* (9), 6132–6140. https://doi.org/10.1039/C6SC01469K.

(54) Goetz, M. K.; Hill, E. A.; Filatov, A. S.; Anderson, J. S. Isolation of a Terminal Co(III)-Oxo Complex. *J. Am. Chem. Soc.* **2018**, *140* (41), 13176–13180. https://doi.org/10.1021/jacs.8b07399.

(55) Aghazada, S.; Miehlich, M.; Messelberger, J.; Heinemann, F. W.; Munz, D.; Meyer, K. A Terminal Iron Nitrilimine Complex: Accessing the Terminal Nitride through Diazo N−N Bond Cleavage. *Angew. Chem. Int. Ed.* **2019**, *58* (51), 18547–18551. https://doi.org/10.1002/anie.201910428.

(56) Valdez-Moreira, J. A.; Beagan, D. M.; Yang, H.; Telser, J.; Hoffman, B. M.; Pink, M.; Carta, V.; Smith,

J. M. Hydrocarbon Oxidation by an Exposed, Multiply Bonded Iron(III) Oxo Complex. *ACS Cent. Sci.* **2021**, *7* (10), 1751–1755. https://doi.org/10.1021/acscentsci.1c00890.

(57) Mao, W.; Fehn, D.; Heinemann, F. W.; Scheurer, A.; Munz, D.; Meyer, K. A Pair of Cobalt(III/IV) Terminal Imido Complexes. *Angew. Chem. Int. Ed.* **2021**, *60* (30), 16480–16486. https://doi.org/10.1002/anie.202103170.

(58) Mao, W.; Fehn, D.; Heinemann, F. W.; Scheurer, A.; Van Gastel, M.; Jannuzzi, S. A. V.; DeBeer, S.; Munz, D.; Meyer, K. Umpolung in a Pair of Cobalt(III) Terminal Imido/Imidyl Complexes. *Angew. Chem. Int. Ed.* **2022**, *61* (36). https://doi.org/10.1002/anie.202206848.

(59) Valdez-Moreira, J. A.; Wannipurage, D. C.; Pink, M.; Carta, V.; Moënne-Loccoz, P.; Telser, J.; Smith, J. M. Hydrogen Atom Abstraction by a High-Spin [FeIII=S] Complex. *Chem* **2023**, S2451929423002395. https://doi.org/10.1016/j.chempr.2023.05.007.

(60) Nieto, I.; Bontchev, R. P.; Ozarowski, A.; Smirnov, D.; Krzystek, J.; Telser, J.; Smith, J. M. Synthesis and Spectroscopic Investigations of Four-Coordinate Nickel Complexes Supported by a Strongly Donating Scorpionate Ligand. *Inorganica Chim. Acta* **2009**, *362* (12), 4449–4460. https://doi.org/10.1016/j.ica.2009.05.015.

(61) Enemark, J. H.; Feltham, R. D. Principles of Structure, Bonding, and Reactivity for Metal Nitrosyl Complexes. *Coord. Chem. Rev.* **1974**, *13* (4), 339–406. https://doi.org/10.1016/S0010-8545(00)80259-3.

(62) Hannigan, S. F.; Lum, J. S.; Bacon, J. W.; Moore, C.; Golen, J. A.; Rheingold, A. L.; Doerrer, L. H. Room Temperature Stable Organocuprate Copper(III) Complex. *Organometallics* **2013**, *32* (12), 3429–3436. https://doi.org/10.1021/om4000538.

(63) Lum, J. S.; Tahsini, L.; Golen, J. A.; Moore, C.; Rheingold, A. L.; Doerrer, L. H. K···F/O Interactions Bridge Copper(I) Fluorinated Alkoxide Complexes and Facilitate Dioxygen Activation. *Chem. - Eur. J.* **2013**, *19* (20), 6374–6384. https://doi.org/10.1002/chem.201204275.

(64) Steele, J. L.; Tahsini, L.; Sun, C.; Elinburg, J. K.; Kotyk, C. M.; McNeely, J.; Stoian, S. A.; Dragulescu-Andrasi, A.; Ozarowski, A.; Ozerov, M.; Krzystek, J.; Telser, J.; Bacon, J. W.; Golen, J. A.; Rheingold, A. L.; Doerrer, L. H. Square-Planar Co(III) in {O $_4$ } Coordination: Large ZFS and Reactivity with ROS. *Chem. Commun.* **2018**, *54* (85), 12045–12048. https://doi.org/10.1039/C8CC04464C.

(65) Brazeau, S. E. N.; Doerrer, L. H. Cu(I)–O $_2$ Oxidation Reactions in a Fluorinated All-O-Donor Ligand Environment. *Dalton Trans.* **2019**, *48* (15), 4759–4768. https://doi.org/10.1039/C8DT05028G.

(66) Elinburg, J. K.; Carter, S. L.; Nelson, J. J. M.; Fraser, D. G.; Crockett, M. P.; Beeler, A. B.; Nordlander, E.; Rheingold, A. L.; Doerrer, L. H. Reversible PCET and Ambient Catalytic Oxidative Alcohol Dehydrogenation by {V=O} Perfluoropinacolate Complexes. *Inorg. Chem.* **2020**, *59* (22), 16500–16513. https://doi.org/10.1021/acs.inorgchem.0c02367.

(67) Dogutan, D. K.; McGuire, R.; Nocera, D. G. Electocatalytic Water Oxidation by Cobalt(III) Hangman β-Octafluoro Corroles. *J. Am. Chem. Soc.* **2011**, *133* (24), 9178–9180. https://doi.org/10.1021/ja202138m.

(68) Dias, H. V. R.; Kim, H.-J.; Lu, H.-L.; Rajeshwar, K.; De Tacconi, N. R.; Derecskei-Kovacs, A.; Marynick, D. S. Investigation of the Electronic and Geometric Effects of Trifluoromethyl Substituents on Tris(Pyrazolyl)Borate Ligands Using Manganese(I) and Copper(I) Complexes. *Organometallics* **1996**, *15* (13), 2994–3003. https://doi.org/10.1021/om9600654.

(69) Albrecht, M. Normal and Abnormal N-Heterocyclic Carbene Ligands. In *Advances in Organometallic Chemistry*; Elsevier, 2014; Vol. 62, pp 111–158. https://doi.org/10.1016/B978-0-12-800976-5.00002-3.

(70) Arduengo, A. J.; Harlow, R. L.; Kline, M. A Stable Crystalline Carbene. *J. Am. Chem. Soc.* **1991**, *113* (1), 361–363. https://doi.org/10.1021/ja00001a054.

(71) Vivancos, Á.; Segarra, C.; Albrecht, M. Mesoionic and Related Less Heteroatom-Stabilized N-Heterocyclic Carbene Complexes: Synthesis, Catalysis, and Other Applications. *Chem. Rev.* **2018**, *118* (19), 9493–9586. https://doi.org/10.1021/acs.chemrev.8b00148.

(72) Dong, Z.; Blaskovits, J. T.; Fadaei-Tirani, F.; Scopelliti, R.; Sienkiewicz, A.; Corminboeuf, C.; Severin, K. Tuning the π-Accepting Properties of Mesoionic Carbenes: A Combined Computational and Experimental Study. *Chem. – Eur. J.* **2021**, *27* (46), 11983–11988. https://doi.org/10.1002/chem.202101742.

(73) Muñoz, S. B.; Foster, W. K.; Lin, H.-J.; Margarit, C. G.; Dickie, D. A.; Smith, J. M. Tris(Carbene)Borate Ligands Featuring Imidazole-2-Ylidene, Benzimidazol-2-Ylidene, and 1,3,4-Triazol-2-Ylidene Donors. Evaluation of Donor Properties in Four-Coordinate {NiNO} ^{10} Complexes. *Inorg. Chem.* **2012**, *51* (23), 12660–12668. https://doi.org/10.1021/ic301204b.

(74) Lee, W.-T.; Dickie, D. A.; Metta-Magaña, A. J.; Smith, J. M. A Tripodal Ligand Constructed from Mesoionic Carbene Donors. *Inorg. Chem.* **2013**, *52* (21), 12842–12846. https://doi.org/10.1021/ic402311c.

(75) Juarez, R. A.; Lee, W.-T.; Smith, J. M.; Wang, H. Computational Evaluation of Tris(Carbene)Borate Donor Properties in {NiNO} ^{10} Complexes. *Dalton Trans* **2014**, *43* (39), 14689–14695. https://doi.org/10.1039/C4DT01426J.

(76) Han, S.; Gao, X.; Wu, Q.; Li, J.; Zou, D.; Wu, Y.; Wu, Y. Transition-Metal-Free Direct Trifluoromethylation and Perfluoroalkylation of Imidazopyridines under Mild Conditions. *Adv. Synth. Catal.* **2019**, *361* (7), 1559–1563. https://doi.org/10.1002/adsc.201801541.

(77) Fan Y.; Cheng J.; Gao Y.; Shi M.; Deng L. Iron Dinitrogen Complexes Supported by Tris(NHC)borate Ligand: Synthesis, Characterization, and Reactivity Study. *Acta Chim. Sin.* **2018**, *76* (6), 445. https://doi.org/10.6023/A18030095.

(78) Huynh, H. V.; Han, Y.; Jothibasu, R.; Yang, J. A. ^{13}C NMR Spectroscopic Determination of Ligand Donor Strengths Using N-Heterocyclic Carbene Complexes of Palladium(II). *Organometallics* **2009**, *28* (18), 5395–5404. https://doi.org/10.1021/om900667d.

(79) Verlinden, K.; Buhl, H.; Frank, W.; Ganter, C. Determining the Ligand Properties of N-Heterocyclic Carbenes from 77Se NMR Parameters. *Eur. J. Inorg. Chem.* **2015**, *2015* (14), 2416–2425. https://doi.org/10.1002/ejic.201500174.

(80) Beerhues, J.; Aberhan, H.; Streit, T.-N.; Sarkar, B. Probing Electronic Properties of Triazolylidenes through Mesoionic Selones, Triazolium Salts, and Ir-Carbonyl-Triazolylidene Complexes. *Organometallics* **2020**, *39* (24), 4557–4564. https://doi.org/10.1021/acs.organomet.0c00614.

(81) Frisch, M. J.; Trucks, G. W.; Schlegel, H. B.; Scuseria, G. E.; Robb, M. A.; Cheeseman, J. R.; Scalmani, G.; Barone, V.; Petersson, G. A.; Nakatsuji, H.; Li, X.; Caricato, M.; Marenich, A. V.; Bloino, J.; Janesko, B. G.; Gomperts, R.; Mennucci, B.; Hratchian, H. P.; Ortiz, J. V.; Izmaylov, A. F.; Sonnenberg, J. L.; Williams-Young, D.; Ding, F.; Lipparini, F.; Egidi, F.; Goings, J.; Peng, B.; Petrone, A.; Henderson, T.; Ranasinghe, D.; Zakrzewski, V. G.; Gao, J.; Rega, N.; Zheng, G.; Liang, W.; Hada, M.; Ehara, M.; Toyota, K.; Fukuda, R.; Hasegawa, J.; Ishida, M.; Nakajima, T.; Honda, Y.; Kitao, O.; Nakai, H.; Vreven, T.; Throssell, K.; Montgomery, J. A., Jr.; Peralta, J. E.; Ogliaro, F.; Bearpark, M. J.; Heyd, J. J.; Brothers, E. N.; Kudin, K. N.; Staroverov, V. N.; Keith, T. A.; Kobayashi, R.; Normand, J.; Raghavachari, K.; Rendell, A. P.; Burant, J. C.; Iyengar, S. S.; Tomasi, J.; Cossi, M.; Millam, J. M.; Klene, M.; Adamo, C.; Cammi, R.; Ochterski, J. W.; Martin, R. L.; Morokuma, K.; Farkas, O.; Foresman, J. B.; Fox, D. J. Gaussian˜16 Revision A.03, 2016.

(82) Becke, A. D. Density-functional Thermochemistry. III. The Role of Exact Exchange. *J. Chem. Phys.* **1993**, *98* (7), 5648–5652. https://doi.org/10.1063/1.464913.

(83) Lee, C.; Yang, W.; Parr, R. G. Development of the Colle-Salvetti Correlation-Energy Formula into a Functional of the Electron Density. *Phys. Rev. B* **1988**, *37* (2), 785–789. https://doi.org/10.1103/PhysRevB.37.785.

(84) Stephens, P. J.; Devlin, F. J.; Chabalowski, C. F.; Frisch, M. J. Ab Initio Calculation of Vibrational Absorption and Circular Dichroism Spectra Using Density Functional Force Fields. *J. Phys. Chem.* **1994**, *98* (45), 11623–11627. https://doi.org/10.1021/j100096a001.

(85) Glendening, E. D.; Landis, C. R.; Weinhold, F. *NBO 6.0* : Natural Bond Orbital Analysis Program. *J. Comput. Chem.* **2013**, *34* (16), 1429–1437. https://doi.org/10.1002/jcc.23266.

(86) Frisch, M. J.; Trucks, G. W.; Schlegel, H. B.; Scuseria, G. E.; Robb, M. A.; Cheeseman, J. R.; Scalmani, G.; Barone, V.; Mennucci, B.; Petersson, G. A.; Nakatsuji, H.; Caricato, M.; Li, X.; Hratchian, H. P.; Izmaylov, A. F.; Bloino, J.; Zheng, G.; Sonnenberg, J. L.; Hada, M.; Ehara, M.; Toyota, K.; Fukuda, R.; Hasegawa, J.; Ishida, M.; Nakajima, T.; Honda, Y.; Kitao, O.; Nakai, H.; Vreven, T.; Montgomery, J. A., Jr.; Peralta, J. E.; Ogliaro, F.; Bearpark, M.; Heyd, J. J.; Brothers, E.; Kudin, K. N.; Staroverov, V. N.; Kobayashi, R.; Normand, J.; Raghavachari, K.; Rendell, A.; Burant, J. C.; Iyengar, S. S.; Tomasi, J.; Cossi, M.; Rega, N.; Millam, J. M.; Klene, M.; Knox, J. E.; Cross, J. B.; Bakken, V.; Adamo, C.; Jaramillo, J.; Gomperts, R.; Stratmann, R. E.; Yazyev, O.; Austin, A. J.; Cammi, R.; Pomelli, C.; Ochterski, J. W.; Martin, R. L.; Morokuma, K.; Zakrzewski, V. G.; Voth, G. A.; Salvador, P.; Dannenberg, J. J.; Dapprich, S.; Daniels, A. D.; Farkas, Ö.; Foresman, J. B.; Ortiz, J. V.; Cioslowski, J.; Fox, D. J. Gaussian∼09 Revision D.01.

(87) Comas-Vives, A.; Harvey, J. N. How Important Is Backbonding in Metal Complexes Containing N-Heterocyclic Carbenes? Structural and NBO Analysis. *Eur. J. Inorg. Chem.* **2011**, *2011* (32), 5025–5035. https://doi.org/10.1002/ejic.201100721.

(88) Soma, S.; Van Stappen, C.; Kiss, M.; Szilagyi, R. K.; Lehnert, N.; Fujisawa, K. Distorted Tetrahedral Nickel-Nitrosyl Complexes: Spectroscopic Characterization and Electronic Structure. *JBIC J. Biol. Inorg. Chem.* **2016**, *21* (5–6), 757–775. https://doi.org/10.1007/s00775-016-1366-7.

(89) Fulmer, G. R.; Miller, A. J. M.; Sherden, N. H.; Gottlieb, H. E.; Nudelman, A.; Stoltz, B. M.; Bercaw, J. E.; Goldberg, K. I. NMR Chemical Shifts of Trace Impurities: Common Laboratory Solvents, Organics, and Gases in Deuterated Solvents Relevant to the Organometallic Chemist. *Organometallics* **2010**, *29* (9), 2176–2179. https://doi.org/10.1021/om100106e.

(90) Pauli, G. F.; Gödecke, T.; Jaki, B. U.; Lankin, D. C. Quantitative ^{1}H NMR. Development and Potential of an Analytical Method: An Update. *J. Nat. Prod.* **2012**, *75* (4), 834–851. https://doi.org/10.1021/np200993k.

(91) Pauli, G. F.; Chen, S.-N.; Simmler, C.; Lankin, D. C.; Gödecke, T.; Jaki, B. U.; Friesen, J. B.; McAlpine, J. B.; Napolitano, J. G. Importance of Purity Evaluation and the Potential of Quantitative ^{1}H NMR as a Purity Assay: Miniperspective. *J. Med. Chem.* **2014**, *57* (22), 9220–9231. https://doi.org/10.1021/jm500734a.

(92) Mahajan, S.; Singh, I. P. Determining and Reporting Purity of Organic Molecules: Why qNMR: Purity by qNMR. *Magn. Reson. Chem.* **2013**, *51* (2), 76–81. https://doi.org/10.1002/mrc.3906.

(93) Beamer, A. W.; Buss, J. A. Synthesis, Structural Characterization, and CO_2 Reactivity of a Constitutionally Analogous Series of Tricopper Mono-, Di-, and Trihydrides. *J. Am. Chem. Soc.* **2023**, *145* (23), 12911–12919. https://doi.org/10.1021/jacs.3c04170.

(94) Kuveke, R. E. H.; Barwise, L.; Van Ingen, Y.; Vashisth, K.; Roberts, N.; Chitnis, S. S.; Dutton, J. L.; Martin, C. D.; Melen, R. L. An International Study Evaluating Elemental Analysis. *ACS Cent. Sci.* **2022**, *8* (7), 855–863. https://doi.org/10.1021/acscentsci.2c00325.

(95) Sheldrick, G. M. *SHELXT* – Integrated Space-Group and Crystal-Structure Determination. *Acta*

Crystallogr. Sect. Found. Adv. **2015**, *71* (1), 3–8. https://doi.org/10.1107/S2053273314026370.

(96) Dolomanov, O. V.; Bourhis, L. J.; Gildea, R. J.; Howard, J. A. K.; Puschmann, H. *OLEX2* : A Complete Structure Solution, Refinement and Analysis Program. *J. Appl. Crystallogr.* **2009**, *42* (2), 339–341. https://doi.org/10.1107/S0021889808042726.

(97) Sheldrick, G. M. Crystal Structure Refinement with *SHELXL*. *Acta Crystallogr. Sect. C Struct. Chem.* **2015**, *71* (1), 3–8. https://doi.org/10.1107/S2053229614024218.

(98) Bhanu Prasad, A. S.; Stevenson, T. M.; Citineni, J. R.; Nyzam, V.; Knochel, P. Preparation and Reactions of New Zincated Nitrogen-Containing Heterocycles. *Tetrahedron* **1997**, *53* (21), 7237–7254. https://doi.org/10.1016/S0040-4020(97)00427-4.

(99) Kawase, M.; Saijo, R.; Kurihara, K. 4-Trifluoroacetyl-2-Phenyloxazol-5-One: Versatile Template for Synthesis of Trifluoromethyl-Substituted Heterocycles. *HETEROCYCLES* **2013**, *87* (12), 2533. https://doi.org/10.3987/COM-13-12838.

Authors are required to submit a graphic entry for the Table of Contents (TOC) that, in conjunction with the manuscript title, should give the reader a representative idea of one of the following: A key structure, reaction, equation, concept, or theorem, etc., that is discussed in the manuscript. Consult the journal's Instructions for Authors for TOC graphic specifications.

Insert Table of Contents artwork here

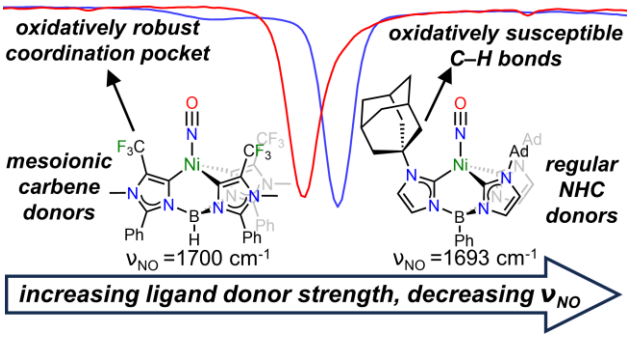

Synopsis: The donor properties of an newly synthesized tris(imidazol-5-ylidene)borate ligand are commensurate to those of alkyl-substituted tris(imidazol-2-ylidene)borates, as indicated by the N–O infrared stretching frequency of each ligands respective $\{NiNO\}^{10}$ complex. The new ligand's fluorinated coordination pocket contrasts with the aliphatic C–H containing coordination pockets of alkyl-substituted tris(imidazol-2-ylidene)borates, which have been shown to be susceptible to deleterious C–H activation by metal-ligand multiply-bonded fragments.